ACS APPLIED OPTICAL MATERIALS

pubs.acs.org/acsaom
Article

Sensitivity Enhancement of a Micro Ring Resonator-Based Photonic Sensor by Using a Gelatin Methacryloyl Functional Coating for the Detection of Metoprolol

Anastasia Tsianaka,[‡] Christian Schweikert,[‡] Alexander Southan,* Niklas Hoppe, Markus Greul, Mathias Kaschel, Wolfgang Vogel,* Manfred Berroth, Georg Rademacher, and Günter E. M. Tovar*

Cite This: https://doi.org/10.1021/acsaom.5c00149
Read Online

ACCESS | Metrics & More | Article Recommendations | Supporting Information

ABSTRACT: Aquatic environments are often contaminated with biopersistent pharmaceuticals, such as the β-blocker metoprolol. The quantitative determination of such pollutants is crucial for environmental monitoring. Therefore, a highly sensitive integrated photonic biosensor for the detection of minute concentrations of metoprolol is presented here. The sensor is based on a thermally robust ring resonator with a hydrogel coating for metoprolol adsorption. Hydrogels consisting of gelatin methacryloyl enabled an increase in the concentration of metoprolol ions in the vicinity of the photonic chip, resulting in high sensitivity of the sensor setup. Compared to an uncoated chip, an increase in sensitivity of up to a factor of 20 was observed. In combination with software-implemented signal processing, the setup showed a detection limit of less than 1×10^{-4} μmol mL^{-1}. The combination of functional coating, thermally insensitive design, and applied digital signal postprocessing makes the system introduced here an attractive approach toward sensor-based wastewater analysis and monitoring.

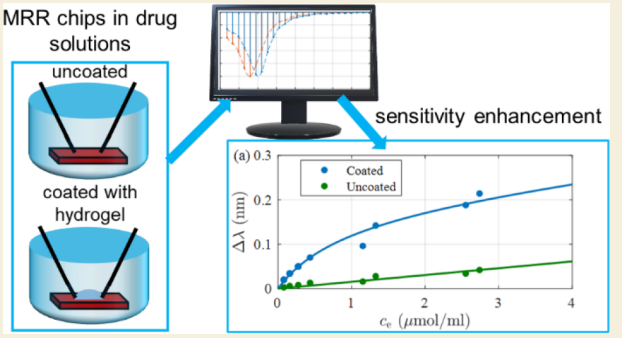

KEYWORDS: *photonic device(s), micro ring resonator, hydrogel, gelatin methacryloyl, adsorption*

INTRODUCTION

Biosensors based on integrated photonic waveguides are of great interest for the detection of a number of different analytes in the environment. Quantitative analysis used for monitoring of the components of aqueous samples from, e.g., wastewater, is a field in which the use of compact photonic biosensors is in high demand. The potential of such sensors for sensitive, scalable, and highly compact point-of-care diagnostics is an advantage compared to commonly used analytical methods, which are time-consuming and require expensive laboratory equipment as well as trained operators. Due to the interaction of the propagating evanescent field with the waveguide's surroundings, small changes of the top cladding's refractive index (RI) cause a proportionally modified phase velocity. By extracting the phase at the end of the sensing waveguide, using, e.g., a resonator, photonic crystal, or interferometer, it is possible to determine the RI of the cladding material that commonly represents the analyte.[1−4] RI changes below 10^{-7} refractive index units (RIU) can be detected by state-of-the art integrated waveguide sensors.[5−7] However, they require sensitivity-optimized photonic waveguide structures, low noise, and accurate measurement equipment as well as isothermal conditions, thus sacrificing the simplicity of the system.

Further improvement of the limit of detection (LoD) of sensors based on integrated photonic waveguides can be realized via functionalizing the waveguides with functional elements, such as biomolecules[8,9] or functionalized polymers with a high affinity for the target analytes. In order to achieve waveguide functionalization, the functional elements are immobilized on the surface of the photonic waveguide chips, mainly by covalent bonds or by strong physical interactions. The functionalization process usually consists of the following steps: First, the surfaces of the photonic chips are cleaned and activated. Then, the surface is primed to allow bonding of the functional elements, for example, by silanization. In the last step of the functionalization, the functional elements are applied as a coating that interacts with the target analytes and leads to an enhancement of the analyte concentration within the coating compared to the surrounding environment.[10,11] Due to this concentration enhancement in the immediate

Received: April 16, 2025
Revised: June 30, 2025
Accepted: July 2, 2025

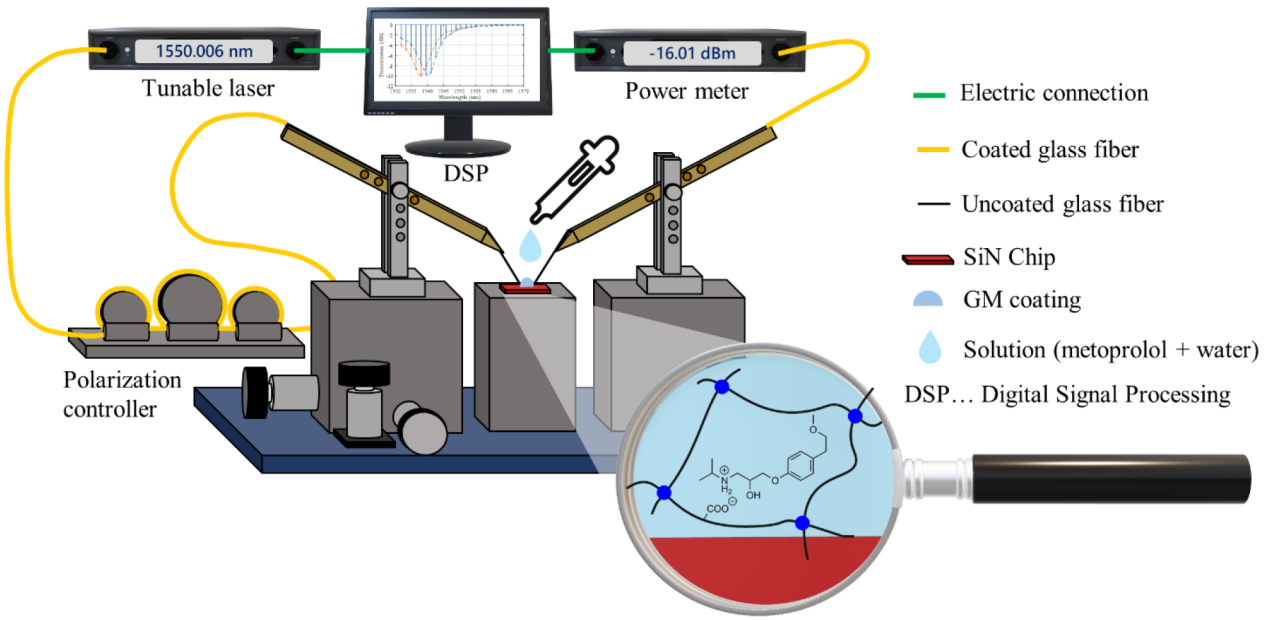

Figure 1. Experimental setup consisting of the photonic chip coated with the GM hydrogel for metoprolol concentration enhancement on the sensor surface. The coated photonic chip is connected to uncoated glass fibers through which the laser light wave is guided. After passing the waveguide, the output power is measured over the experimental wavelength range. When metoprolol is present in the solution, it adsorbs on the GM hydrogel due to electrostatic interaction. For a more detailed view of the hydrogel, see Figure S1, Supporting Information.

surroundings of the waveguide, the evanescent field sees an effectively larger concentration that correlates linearly with the RI.

Functional coatings consisting of (bio)polymers have been successfully applied as sensitive elements for optical sensors.[12,13] In contrast to sensors functionalized with a monolayer of immobilized antibodies, functionalization with a three-dimensional polymer coating can offer increased binding capacities as well as flexibility regarding the binding of analytes.[14] For example, Hoppe et al. functionalized a dual-mode interferometer (DMI) with a thin layer of imprinted poly(MMA-*co*-EGDMA) for the detection of L-Boc-phenylalanin anilid (L-BFA).[15] The functionalization led to a pronounced phase shift due to selective L-BFA adsorption on the imprinted polymer and thus to enhanced sensitivity of the chip. The study also showed that even a nonimprinted poly(MAA-*co*-EGDMA) coating led to an enhanced phase shift compared to the nonfunctionalized DMI, which was attributed to nonspecific adsorption of the analyte on the polymer coating. Nonspecific interactions of the analytes with functional building blocks of the polymer can thus be used as an alternative to specific interactions.

Hydrogels, polymer networks that are swollen in water,[16] are promising candidates as functional coatings for sensing in aqueous solutions. Hydrogels have already found application in sensing,[17,18] as adsorbers,[19,20] and also in fields like drug delivery[21−23] or tissue engineering.[24,25] The easy diffusion of analytes throughout the polymer network[26] combined with the relatively easy introduction of building blocks with certain functionalities[27−29] enables the enrichment of analytes in the hydrogel bulk. For example, by incorporating building blocks with positively or negatively charged groups in the polymer network, the adsorption of charged analytes is possible. The adsorption of various analytes on hydrogels has been the object of various studies and has been accurately described by known adsorption models, like Langmuir or Freundlich.[30−32] Examples include the adsorption of metal ions[33,34] of organic dyes[35,36] and of common drugs like diclofenac and metoprolol.[37−39] Despite the numerous studies on analyte adsorption on hydrogels, most of them are focused solely on the materials as adsorbers and not on the effect that the analyte enrichment has on the material properties and the possible applications that arise from that.

The significant increase of analyte concentration in the hydrogel leads to changes of key physical properties of the hydrogels that are crucial for sensing applications.[40] As mentioned, an important physical property with regard to optical sensors based on photonic structures is the RI. It is thus important to correlate the concentration enhancement of analytes in the hydrogel caused by adsorption to refractive index changes. Previous work has shown that the Langmuir-type adsorption of the drugs diclofenac sodium and metoprolol tartrate on functionalized poly(ethylene glycol) diacrylate (PEG-DA) hydrogels led to a defined increase of the refractive index of the hydrogels of around 10^{-3} RIU with increasing drug concentration in the hydrogels.[38] In that work, concentration enhancement factors >1000 were observed for diclofenac and >10 for metoprolol, highlighting the importance of the material choice to maximize potential sensor response.

In the present work, we demonstrate the sensitivity enhancement of photonic biosensors based on a functional coating. For this purpose, a gelatin methacryloyl (GM) hydrogel is used that is able to interact with the target ionic drug metoprolol. Metoprolol is one of the most frequently detected β-blockers in the environment with concentrations up to 3×10^{-4} μmol mL^{-1} in wastewater influents.[41] For material characterization, metoprolol adsorption in bulk GM hydrogels is measured. Subsequently, a micro ring resonator (MRR) in the 250 nm silicon nitride technology that serves as sensitive photonic device is coated with a GM hydrogel, as shown in Figure 1. For reliable measurement, the MRR is designed for a thermally insensitive operation. The uncoated and coated

https://doi.org/10.1021/acsaom.5c00149
ACS Appl. Opt. Mater. XXXX, XXX, XXX−XXX

MRR were calibrated by measuring aqueous metoprolol solutions with different concentrations. A comparison of the results enables computation of the enhancement effect induced by the used GM hydrogel coating. Also, a digital signal processing algorithm of the detected signals is demonstrated for further sensitivity improvement.

EXPERIMENTAL SECTION

Materials

Metoprolol tartrate (≥98%), methacrylic anhydride (≥94%), lithium phenyl-(2,4,6-trimethyl benzoyl)phosphinate (LAP), 4-morpholineethanesulfonic acid (≥99%, MES), 4-morpholineethanesulfonic acid sodium salt (≥99%, MES-Na), and trifluoroacetic acid (suitable for HPLC, ≥99%, TFA) were purchased from Sigma-Aldrich (Darmstadt, Germany). Gelatin type B (232 blooms) was donated by Gelita (Eberbach, Germany). (3-Methacryloxypropyl) dimethyl chlorosilane (92%) was purchased from abcr GmbH (Karlsruhe, Germany). Acetonitrile (ROTISOLV HPLC gradient grade) was purchased from Carl Roth GmbH + Co. KG (Karlsruhe, Germany). Ethanol (absolute, ≥99.5%, EMPLURA, Supelco) was purchased from VWR International GmbH (Darmstadt, Germany). Deionized water was obtained through a TKA X-CAD ultrapure water purification system from TKA Wasseraufbereitungssysteme GmbH (Niederelbert, Germany). MES buffer (20 mM) for HPLC was obtained by dissolving 10 mmol of MES and 10 mmol of MES-Na in water in a 1 L volumetric flask.

Photonic Device Fabrication and Characterization

The photonic devices were fabricated on 150 mm silicon substrates with 3 μm buried oxide and a 250 nm-thick silicon nitride layer by IMS CHIPS (Stuttgart, Germany). The device patterns were transferred by electron beam lithography and dry etching processes. First, the grating layer was exposed to a positive tone resist and etched 160 nm deep into the nitride layer. Then, the waveguides were patterned using a negative tone resist and etching 250 nm deep to the buried oxide. Every processing step was followed by a subsequent inspection for process control monitoring and wafer cleaning routines. After waveguide patterning, a 1080 nm-thick cladding oxide was deposited by using low pressure chemical vapor deposition. The cladding oxide was then back-thinned to 100 nm using hydrofluoric acid.

The photonic devices were characterized by the setup illustrated in Figure 1. The optical signal is coupled from the laser (Agilent 81682A TLS in 8164B mainframe) into a single-mode fiber (SMF 28). The laser is tunable in a spectral range from 1460 to 1580 nm with a spectral resolution up to 0.1 pm. A subsequent polarization controller (Thorlabs model FPC031) enables a defined setting of polarization. Over grating couplers, the optical signal is diffracted from the fiber into the waveguide layer of the photonic chip. Therefore, the fiber is uncoated and spliced at its open end. A self-made holder enables the alignment of the diffraction angle between the fiber and the chip that is designed to around 15° for a wavelength of 1550 nm. With the same chip-to-fiber interface, the light is guided to the powermeter (Agilent 81619A Powermeter in 8164B mainframe) that is triggered to the laser source and connected to a computer with a GPIB interface. The temperature is controlled by a TEC Controller Starter Kit SKT-1165 from Meerstetter with an accuracy of 0.01 K.

Gelatin Methacryloyl Synthesis

GM was synthesized as described before.[42,43] Briefly, 100 g of gelatin were dissolved in 1000 mL of ultrapure water at 40 °C. After adjusting the pH to 7.25 using an automatic titrator, 53.96 g methacrylic anhydride were added slowly and the mixture was stirred for 5 h. The amount of added methacrylic anhydride corresponded to a 10-fold molar excess compared to the amino groups of gelatin.[43] After the reaction, the pH was adjusted to 9.5, and the mixture was filtered using a bottle top filter and stored at 4 °C for 2 days. The pH of the mixture was adjusted to 9.5 again, and the mixture was purified using cross-flow filtration. Subsequently, the solution was lyophilized and the degree of methacrylation was determined by ^{1}H NMR spectroscopy using the method described by Claaßen et al.[44] In the present work, GM with degrees of methacrylation of 0.87 ± 0.03 and 1.14 ± 0.02 mmol g^{-1} was used. The corresponding ^{1}H NMR spectra are shown in Figure S2 in the Supporting Information.

Hydrogel Preparation

The hydrogel precursor solutions were prepared by dissolving appropriate amounts of GM and the photoinitiator LAP in ultrapure water. The obtained solutions contained 10% (w/w) GM and 0.05% (w/w) LAP. In detail, 2 mg of LAP were mixed with 3.598 g of ultrapure water and shaken. To this solution, 0.400 g GM were added. The mixture was shaken at room temperature until all components were dissolved. Hydrogels for batch adsorption experiments were prepared by pipetting 750 μL of the precursor solution in cylindrical molds with a diameter of 30 mm and a depth of 1 mm, covered with a quartz glass pane and cured for 7.5 min in a UV chamber (Sol2, Dr. Hönle AG, Germany) at an intensity of 50 mW cm^{-2}. The cured hydrogels were removed from the molds, and smaller samples with a diameter of 8 mm each were punched out. The hydrogel samples were weighed for the mass m_H and subsequently washed in ultrapure water for 24 h to remove any unreacted components.

Batch Adsorption Experiments

Prior to using the GM hydrogels as sensor coatings, the adsorption behavior of metoprolol on the GM hydrogels was characterized by batch adsorption experiments. For this purpose, each hydrogel under test was submerged in a metoprolol solution with volume V_0 = 4 mL and a given initial concentration c_0 for a defined adsorption time t_{ads}. It should be noted that all metoprolol concentrations in this contribution pertain to the metoprolol ion, of which one mol of metoprolol tartrate contains two moles. The adsorption was carried out under gentle agitation on a shaker at 45 rpm at 25 °C. The supernatants were then collected and the metoprolol concentrations c_{met} (in the supernatant) and c_0 were measured by high-performance liquid chromatography (HPLC), a common analytical method used for both quantitative and qualitative analysis of solutes.[45] For this, a Shimadzu Prominence HPLC-System (Shimadzu Deutschland GmbH, Germany) with a ReproSil Gold 120 C4 column (5 μm, 150 × 4.6 mm, Dr. Maisch GmbH, Germany) was used. All measurements were conducted at 40 °C with an isocratic flow of 1 mL min^{-1}. The eluent consisted of 30% acetonitrile and 70% 20 mM MES buffer (pH = 6.0). The evaluation of all chromatograms was carried out by integrating the metoprolol peak resulting from UV absorption at a wavelength of 274 nm. The metoprolol concentrations were calculated using a previously prepared calibration curve. The amount q of adsorbed metoprolol was calculated by the following equation:

$$q = \frac{(c_0 - c_{met})V_0}{m_H} \quad (1)$$

First, adsorption kinetics measurements were conducted with c_0 = 0.292 μmol mL^{-1} and t_{ads} between 0 and 4320 min in order to determine the adsorption time t_e when the equilibrium values c_e and q_e of c_{met} and q, respectively, were reached. After that, the adsorption isotherm was measured by submerging the hydrogels for t_e = 72 h in metoprolol solutions with various values of c_0 (0.146, 0.292, 0.584, 1.168, 2.336, and 4.381 μmol mL^{-1}). The resulting c_e values were used to calculate the respective q_e values by using eq 1.

The calculated values were fitted using an extended Langmuir model for adsorption, which takes the aqueous phase in the hydrogel into account[46] under the assumption that the metoprolol concentration in the aqueous phase within the hydrogel is the same as the equilibrium concentration in the supernatant:[47]

$$q_e = \frac{c_e \cdot \phi_H}{\rho_H} + q_m \frac{K_s \cdot c_e}{1 + K_s \cdot c_e} \quad (2)$$

ϕ_H is the volume fraction of water in the hydrogel and ρ_H is the density of the hydrogel. Since the GM hydrogels consist mainly of water, it is approximated that the density is similar to water (ρ_H = 1 g

https://doi.org/10.1021/acsaom.5c00149
ACS Appl. Opt. Mater. XXXX, XXX, XXX−XXX

mL^{-1}). A water volume fraction of $\phi_H = 0.9651$ was determined using the equilibrium degree of swelling (see eqs S2 and S3, Supporting Information). The fit parameters q_m and K_s are the maximum adsorption capacity of the hydrogel and the ratio of the adsorption and desorption rate constants, respectively. K_s is a measure of the affinity of the solute for the hydrogel.

Using the determined q_e values, the enhancement factor E that describes the ratio of the ideal and the real partition coefficients can be calculated using[48]

$$E = \frac{q_e \cdot \rho_H}{c_e \cdot \phi_H} \tag{3}$$

Coating of the Ring Resonator Chips

Prior to coating, the ring resonator chips were functionalized with a silane that enables covalent bonding of the GM. For this purpose, the chips were cleaned with acetone, isopropanol, and ultrapure water and dried using nitrogen gas. Subsequently, the wafers were placed in 60 mL of ethanol containing 300 μL of (3-methacryloxypropyl)-dimethylchlorosilane and shaken for 1 h at 45 rpm. Subsequently, the functionalized chips were washed with ethanol and dried using nitrogen gas. The ring resonator chips were coated with 1.5 μL of the 10% (w/w) GM solution containing 0.05% (w/w) LAP, as described above, using an air displacement micropipette. For this, the chips were placed under a microscope, and the GM solution was pipetted over the ring resonator and directly cured using a UV flashlight (Alonefire SV13, 15 W, 365 nm) for 25 s. In addition to the waveguide chips, unstructured silicon chips (without waveguides) were also silanized and coated in order to determine the ideal adsorption equilibrium conditions for the coatings.

Chip and Sensor Calibration (with Aqueous Metoprolol Solutions)

In order to determine the effect of the GM coating on the measured shift of the waveguide spectrum, the coated chip was immersed in solutions containing different metoprolol concentrations. First, the chip was immersed in 20 mL of ultrapure water. Multiple spectra were recorded for a period of 20 min to ensure that an adsorption equilibrium is reached. Afterward, the water was removed and the waveguide chip was immersed in 20.2 mL of a 0.087 μmol mL^{-1} metoprolol solution and the spectra recorded again. Subsequently, appropriate amounts of a metoprolol stock solution (c_{Stock} = 5.841 μmol mL^{-1}) were consecutively added in order to obtain a solution with a specific metoprolol concentration (listed in Table S1, Supporting Information). After each addition, the spectra were recorded for 20 min. Samples with the same concentrations were prepared at the same time for accurate determination of the concentration via HPLC. The same process was repeated with a waveguide chip without a GM coating.

RESULTS AND DISCUSSION

Photonic Device Design for Sensing

In this study, an MRR manufactured in a 250 nm silicon nitride photonic device platform enables the analysis of metoprolol concentrations in aqueous solutions. Due to their compact dimensions, MRRs are particularly well-suited for integration into highly dense and complex arrays. Its fundamental principle is illustrated in Figure 2a. First, a wave couples via a grating coupler into the waveguide. Upon a direction coupler with a transmission coefficient of t, the electric field is partially coupled evanescently into the waveguide of the ring. After a round-trip, the electric field magnitude is damped to α_r, before it passes the coupling section again. In the stationary case, its transmission $\mathcal{T}$, i.e., the output power P_{out} divided by the input power P_{in}, results in

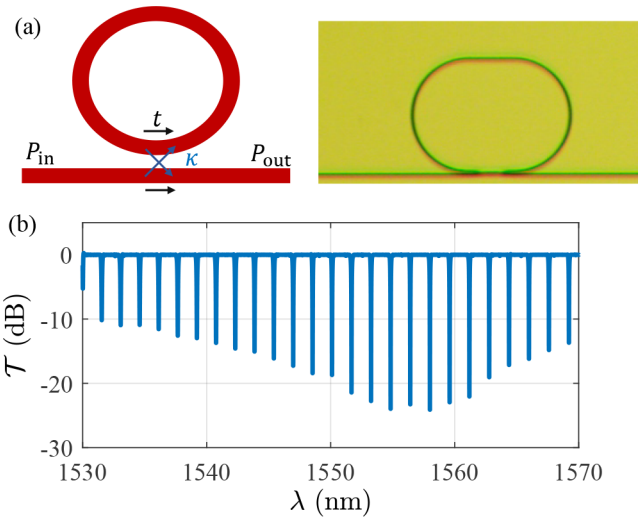

Figure 2. (a) The functionality and a micrograph of a ring resonator in all-pass configuration. (b) The measured spectral transmission of an MRR that is coated by the GM hydrogel.

$$\mathcal{T} = \frac{P_{out}}{P_{in}} = \frac{t^2 + \alpha_r^2 - 2t\alpha_r \cos\left(\frac{2\pi}{\lambda} n_{eff} L\right)}{1 + t^2\alpha_r^2 - 2t\alpha_r \cos\left(\frac{2\pi}{\lambda} n_{eff} L\right)} \tag{4}$$

Dependent on the phase that composes of the geometrical length of the ring L, the wavelength λ, and the effective refractive index n_{eff}, resonances occur in the transmission spectrum. A change in the metoprolol concentration of the waveguide cladding will result in a corresponding alteration of n_{eff}. This, in turn, will induce a shift in the phase and a movement of the resonances across the wavelength. Figure 2b shows an exemplary measured spectral transmission of an 800 μm-long Si_3N_4 ring resonator with a 1 μm wide slab waveguide that is coated by a GM hydrogel.

A crucial figure of merit of an MRR is represented by the bulk sensitivity. It defines the sensor response caused by changes of the analyte concentration c in the cladding material:

$$S_c = \frac{\lambda}{n_g} \frac{\partial n_{eff}}{\partial c} \tag{5}$$

with n_g being the group index of the guided ring mode. In general, the larger the evanescent field of the guided mode, the better the sensitivity. However, in the present device, we implemented a 100 nm-thin passivation between the sensitive sensing waveguide and the hydrogel that reduces the evanescent fields and thus the sensitivity by a factor of 0.6. The reason for the passivation is the reduction of the thermal influence. Fluctuations in temperature affect the device in the same way as the concentration changes: a spectral shift dependent on the thermal sensitivity.

$$S_T = \frac{\lambda}{n_g} \frac{\partial n_{eff}}{\partial T} \tag{6}$$

While silicon nitride and silicon dioxide have thermo-optic coefficients (TOCs) of 2.4×10^{-5} RIU/K and 0.8×10^{-5} RIU/K, respectively, water shows a negative TOC of -1.1×10^{-4} RIU/K.[49,50]

Therefore, a geometry should be found with matched evanescent and confined field parts that effectively suppresses a thermal impact.

https://doi.org/10.1021/acsaom.5c00149
ACS Appl. Opt. Mater. XXXX, XXX, XXX−XXX

Figure 3a illustrates a simulation for a water-cladded, a SiO_2-cladded, and a 100 nm-thin- silicone dioxide-water-cladded

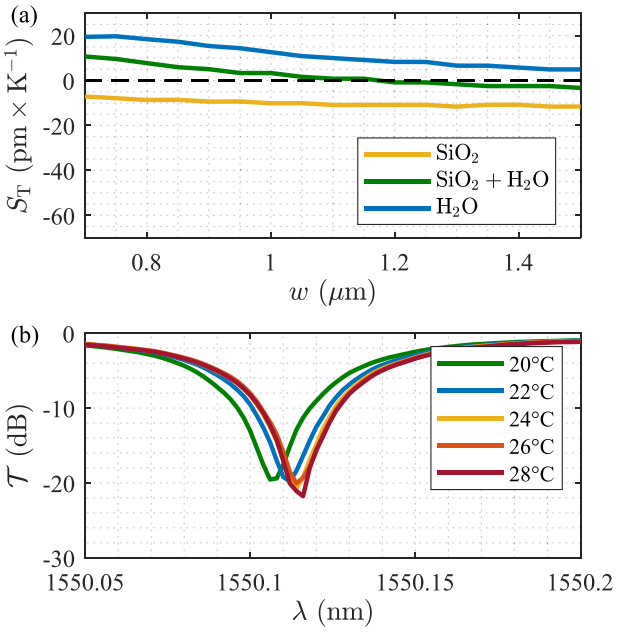

Figure 3. (a) The simulation of the thermal sensitivity S_T dependent on the waveguide width. (b) The thermal characterization of an MRR with a 100 nm passivation between the 1 μm wide slab waveguide and the GM hydrogel.

slab waveguide with different waveguide widths by an alternating temperature around 24 °C for TE polarization. A thermal insensitive waveguide can only be reached with a passivation in the aspired monomodal slab waveguide geometry. According to simulation, this athermal geometry is at a width of 1.150 μm. The width of 1 μm was selected on the basis that the properties of the gel are only approximate to those of water. A thermal characterization of the fabricated MRR in Figure 3b implies a thermal sensitivity of $S_T \sim 1$ pm/K that matches with the simulation in Figure 3a. Consequently, temperature fluctuations of ΔT during the measurement result in undesired wavelength shifts of $S_T \Delta T$. Together with the spectral resolution of the tunable laser ρ_λ, a measurement uncertainty can be determined. This, in turn, affects the most crucial parameter of a sensor, namely, its limit of detection:

$$\mathrm{LoD} = 3\frac{\sqrt{(S_T \Delta T)^2 + \rho_\lambda^2}}{S_c} \tag{7}$$

Adsorption Isotherms of GM Hydrogels

After designing the photonic device for sensing, the next step toward building the sensor prototype shown in Figure 1 was to identify a suitable coating material for metoprolol concentration enhancement. Gelatin methacryloyl is a versatile biopolymer obtained through collagen hydrolysis that has been used extensively in fields like bioprinting and tissue engineering,[51−53] drug delivery,[28,54] and also biosensing.[17,55] Its chemical and physical properties, such as the cross-linking mechanism and rheological properties, have been extensively described in the literature.[56−58] As first reported by Nazarova et al. and then by Van Den Bulcke et al., GM is obtained through the reaction of the amine and hydroxyl residues of gelatin with methacrylic anhydride.[43,59] Depending on the available amount of methacrylic anhydride during functionalization, the degree of modification can be adjusted. If methacrylic anhydride is offered in a high molar excess during functionalization, then a GM with a high degree of modification is obtained. In this case, all amine residues are substituted and the net charge of GM is negative in near neutral aqueous solution due to the carboxyl groups present on gelatin.[60] GM hydrogels, obtained through photoinduced cross-linking of the methacryloyl groups are thus good candidates for the adsorption of positively charged analytes such as metoprolol.[39]

The hydrogels were prepared by irradiating GM solutions containing the photoinitiator LAP with UV light, as described in the experimental section. The cross-links were formed between the methacryloyl groups through a radical polymerization. The success of the cross-linking was confirmed by the average yield of the obtained hydrogels which was 106.8 ± 4.5% (see eq S4, Supporting Information). The high yield indicates a quantitative incorporation of all of the polymer present in the solution into the polymer network through cross-linking. The average yield being higher than 100% can be attributed to residual water which was not removed during the drying process. Similar yields have been obtained in the past for hydrogels prepared with GM with similar degrees of methacrylation.[58] The successful conversion of the methacryloyl groups was also determined by comparing Raman spectra of the cross-linked hydrogels to spectra of pristine GM, which are shown in Figure S3 and discussed in the Supporting Information.

In order to determine the way the GM interacts with the ionic drug metoprolol tartrate and to describe the response of the hydrogel, the adsorption behavior of metoprolol was investigated by batch adsorption experiments. Adsorption kinetics measurements showed that a stable time-independent metoprolol concentration c_e in the supernatant was reached between 48 and 72 h adsorption time t_{ads}, indicative of adsorption equilibrium (see Figure S4, Supporting Information). The adsorption isotherm of the GM is shown in Figure 4a. The adsorbed amount of q_e of metoprolol increased with increasing equilibrium concentration c_e. At low c_e, the increase of q_e was steeper, whereas at higher c_e, a flattening of the curve was observed, while no plateau was reached in the observed range of equilibrium concentrations. Under the assumption that all adsorption sites in GM are accessible and thus available for all metoprolol ions and that each metoprolol ion can adsorb only on one adsorption site, the data was fitted with the modified Langmuir model of adsorption given by eq 2. Through the fit, parameters q_m and K_s were determined. The obtained values were q_m = 79.7 μmol g^{-1} and K_s = 0.56 mL μmol^{-1}. The enhancement of metoprolol in the GM hydrogels was significant, as indicated by the calculated enhancement factors E, shown in Figure 4b. The highest enhancement factors with values above 60 were calculated for low amounts of adsorbed metoprolol, whereas with increasing q_e the enhancement factor values decreased, which is in accordance with the used Langmuir model of adsorption given by eq 2. The high enhancement at low drug concentrations is crucial for the use of the GM as a material for sensing. Another crucial aspect is the ability to regenerate the material for repeated sensor use. This is the case for GM hydrogels, for which high desorption rates have been achieved.[39] It has been shown that the adsorption of charged drugs like metoprolol on other polyelectrolyte hydrogels based on PEG-DA lead to defined

https://doi.org/10.1021/acsaom.5c00149
ACS Appl. Opt. Mater. XXXX, XXX, XXX−XXX

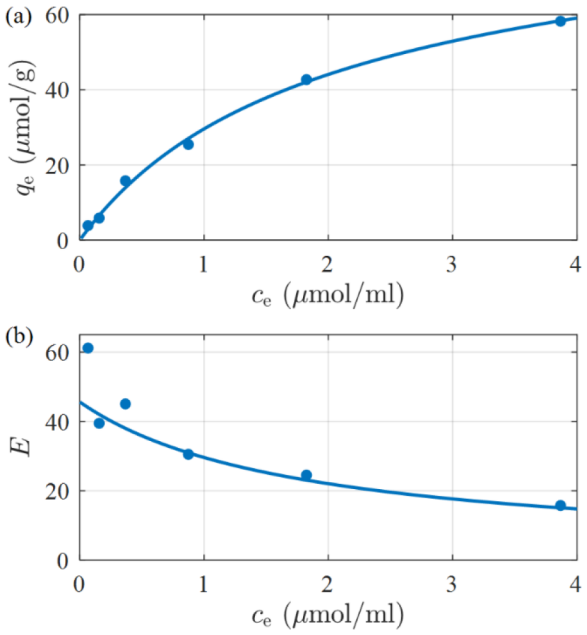

Figure 4. (a) Adsorption isotherm of GM hydrogels with the solute metoprolol. The individual data points are the measured equilibrium concentrations c_e of metoprolol in the supernatant at a certain concentration q_e of metoprolol within the GM hydrogels. The data was fitted with the extended Langmuir model of adsorption (eq 2). (b) Enhancement factors E of the GM hydrogels as a function of c_e. The blue curve was calculated with eq 3 with the fit parameters obtained from the Langmuir model of adsorption.

changes of the refractive index in the hydrogel with E values around 10.[38] Given the higher E values for the GM hydrogels, their use as functional coatings for sensitivity enhancement of photonic devices, whose working principle is based on RI differences in the cladding, should be possible. The Langmuir adsorption model, which in this case describes the response of the hydrogel to the presence of metoprolol in an aqueous solution, can be used to correlate the concentration in the hydrogel to the phase changes detected by the photonic device.

MRR Coating with GM and Adsorption Equilibrium Conditions

In contrast to the adsorption experiments described above with macroscopic hydrogels with a dimeter of 8 mm and a thickness of approximately 1 mm, the GM hydrogel sensor spots had a much smaller volume of 1.5 μL. This was expected to lead to two main differences: First, the amount of adsorbed metoprolol per spot will be much smaller, leading to a very small concentration change ($\Delta c = c_0 - c_e$) of the supernatant solution. Second, the time to reach equilibrium conditions will be much shorter due to smaller diffusion lengths through the gel matrix.[39]

Concerning the concentration change, for using the envisioned system as a sensor, it is crucial that Δc is as small as possible in order to avoid a large influence of the sensor on the measured solution. The magnitude of Δc can be estimated by combining eqs 1 and 2 and solve for c_e with a given c_0 and V_0 together with the fit results of the adsorption isotherm. With a realistic parameter set (c_0 = 0.292 μmol mL^{-1}, V_0 = 20 mL) for the sensing experiments below, this would result in c_e = 0.291 μmol mL^{-1}. This corresponds to a very small Δc of 0.001 μmol mL^{-1}, and such a small change is expected to be under the limit of detection of common methods, such as HPLC and UV−vis spectroscopy. In order to further elaborate on this, coated unstructured silicon chips were tested experimentally by HPLC under the given conditions. As Figure 5 shows, no trend in the measured metoprolol

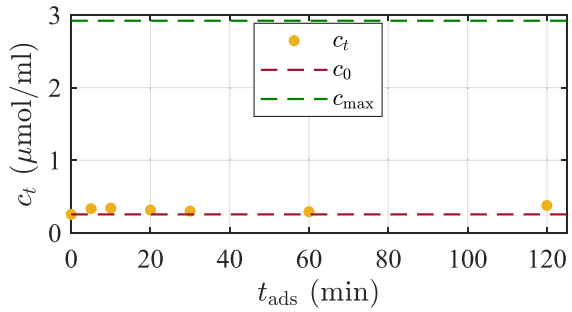

Figure 5. Supernatant metoprolol concentrations c_t as a function of adsorption time t_{ads}, obtained with GM-coated unstructured Si chips in contact with a metoprolol solution of the concentration c_0 = 0.292 μmol mL^{-1} and volume V_0 = 20 mL. For comparison, the line that represents the highest metoprolol concentration c_{max} used for the experiments is also shown.

concentration in the supernatant was observed, and the measured concentrations stayed close to c_0. Thus, we conclude that the spot size is sufficiently small to allow sensor usage also in relatively small sample volumes.

The small Δc however also means that it is not possible to use HPLC to measure the necessary time to reach equilibrium. However, ensuring that all measurements are conducted in equilibrium is a prerequisite to accurately describe the relationship between changes in the transmission spectrum of the photonic device and the metoprolol concentration in solution. Therefore, the time to reach equilibrium conditions was measured directly with ring resonator chips (see description in the next section). This showed that after 20 min of adsorption time a stable state was reached, which leads to the conclusion that equilibrium conditions were achieved. These observations led to the experimental method for the sensor prototype calibration used in this work.

As the next step, the photonic chips were coated with the GM precursor solution and cured for 25 s using a UV flashlight. After curing, a GM hydrogel coating in the shape of a circular spot was obtained (see Figures S5 and S6, Supporting Information). Through surface modification with silane, the GM spot was covalently bound on the chip. The covalent bond was stable, as the coating did not detach after the chip was placed in water, even after several days of shaking. Measurements with a digital caliper showed an average thickness of the swollen coatings of 153 ± 12 μm, while the dried coatings had a thickness around 30 μm (Figure S6, Supporting Information).

Sensor Calibration

For the determination of the effect that the hydrogel coatings have on the phase of the wave coupled in the waveguide and in turn on the resonances in the obtained transmission spectra, a calibration of both coated and uncoated MRR chips with different metoprolol solutions is crucial. For this, the previously characterized MRR chip was placed − first uncoated and then coated with a GM hydrogel − in ultrapure water and various metoprolol solutions with defined concentrations. The obtained transmission spectra of both uncoated and coated chips showed a shift of the resonances toward higher

https://doi.org/10.1021/acsaom.5c00149
ACS Appl. Opt. Mater. XXXX, XXX, XXX−XXX

wavelengths in the presence of metoprolol (see Figure S7, Supporting Information). With increasing metoprolol concentration, the shifts observed in the spectra measured with the coated MRR chip were notable. The shifts measured with the uncoated chip were overall lower, especially for the solutions with very low metoprolol concentrations, as shown in Figure 6a. The comparison between the obtained wavelength shifts

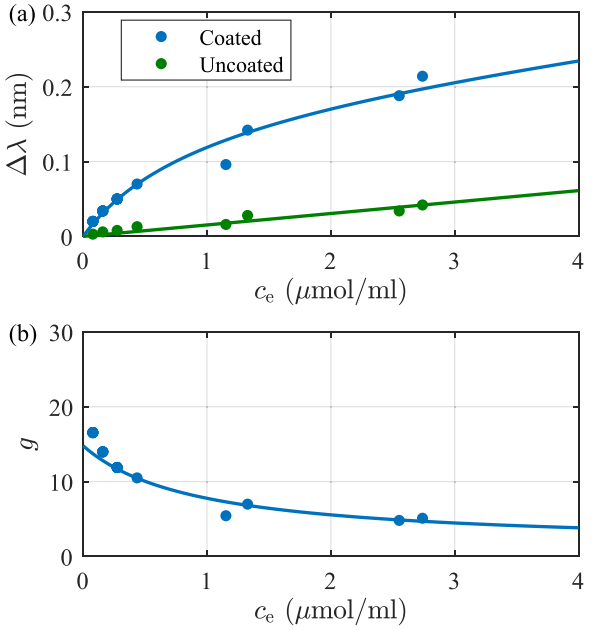

Figure 6. (a) The measured wavelength shifts $\Delta\lambda$ as a function of the equilibrium concentration of metroprolol c_e in the surrounding of the MRR's evanescent field and (b) the resulting gain factor g of the GM hydrogel.

$\Delta\lambda$ for coated and uncoated chips illustrates the enhancement effect of the GM hydrogel coating. For the uncoated chips, a linear relationship between $\Delta\lambda$ and c_e was observed, as expected for low concentrations, which can be described by the following equation:[38,61]

$$\Delta\lambda = S_c \cdot c_e \tag{8}$$

The slope S_c of the measured, green curve corresponds to the concentration sensitivity, which we determined by linear regression to be S_c = 15 pm ml μmol^{-1}. The measured shift data of the coated chip form a curve similar to the adsorption isotherm measured for GM hydrogels (Figure 4(a)). Such a behavior confirms that the working principle of the functional coating is based on the described adsorption behavior of the GM hydrogels. At low concentrations, a steep, almost linear increase of the concentration of metoprolol in the hydrogel coating takes place. As the adsorption sites get consecutively occupied by metoprolol ions with increasing metoprolol concentration in the surrounding medium, there are less sites available. This leads toward a saturation in the hydrogel, which in turn leads to smaller changes of its optical properties and thus to lower spectral shifts. In the tested concentration range, no full saturation was achieved, as evidenced by both the adsorption isotherm and the obtained shifts. Thus, a detection of unknown metoprolol concentrations should be possible in the tested concentration range with the proposed sensor prototype. For this, a function that describes the sensor's response to a metoprolol solution concentration can be set up.

If the MRR is coated, the waveguide sees the metoprolol concentration in the hydrogel, which compared to the solution concentration is enhanced by factor g:

$$\Delta\lambda = S_c \cdot g \cdot c_e \tag{9}$$

The gain factor g is indicative of the enhancement effect the GM coating has on the wavelength shift, and it is thus also dependent on the metoprolol adsorption. This is also evident upon comparison of the obtained curve, shown in Figure 6b to the curve obtained for the enhancement factor E (Figure 4b). However, g cannot be directly compared to E. The highest obtained g values were just below 20, which is 3-fold lower than the obtained values for E. These discrepancies suggest that even though metoprolol adsorption has a major effect on the spectral shifts, there are also other adsorption-adjacent effects that determine the values of g. Possible reasons for the observed discrepancies could be deviations at room temperature or curing. We hypothesize, however, that the major reason is a change of the equilibrium degree of swelling of the GM spots as a function of metoprolol adsorption. It was reported previously for example that the refractive index of a polyelectrolyte hydrogel did not change much upon diclofenac adsorption, and the authors attributed this to a difference in swelling.[38]

Taking the functionalization into account, the LoD for the concentration of metoprolol results in

$$\mathrm{LoD}_c = 3\frac{\sqrt{(S_T \Delta T)^2 + \rho_\lambda^2}}{g S_c} \tag{10}$$

With a minimal spectral step size of the laser source of 0.1 pm and a thermal stability of ΔT = 0.01 K of the used TEC, the LoD is enhanced from 0.02 μmol mL^{-1} to 0.001 μmol mL^{-1} due to the enhancement of the functionalization.

Sensitivity-Enhancement Using Digital Signal Processing (DSP)

To further improve the performance of the system, a better resolution of the measurement equipment or a larger sensitivity of the photonic device is required that, e.g., can be achieved by other waveguide cross sections like slot waveguides or sublambda structures. We propose a preprocessing of the measured data.[62] First, the measurement data is processed by filtering, fitting,[63] and scaling to a constant value of −10 dB. Then, the free spectral ranges $\mathrm{FSR_R}$ of the resonances are extracted. As the next step, an envelope is generated by sampling the calibrated measurement data. The selected discrete sampling wavelengths can be described as a frequency comb with a free spectral range $\mathrm{FSR_S}$. A further consideration is the shift of the envelope rather than the shift of the resonances. This reveals a larger wavelength shift that is enhanced by the factor of

$$K = \frac{\mathrm{FSR_S}}{|\mathrm{FSR_R} - \mathrm{FSR_S}|} = \frac{\mathrm{FSR_S}}{\Delta\mathrm{FSR}} \tag{11}$$

Figure 7 shows a demonstration. The measurement of a small wavelength shift of 15 pm, see Figure 7a, serves as the initial point. Dependent on these extracted FSR_R, a digital frequency comb is constructed with the free spectral range of

$$\mathrm{FSR_S} = \mathrm{FSR_R} - \Delta\mathrm{FSR} \tag{12}$$

This comb is shifted in the spectra so that it perfectly overlaps with an arbitrary chosen resonance at 1537.964 nm of

https://doi.org/10.1021/acsaom.5c00149
ACS Appl. Opt. Mater. XXXX, XXX, XXX−XXX

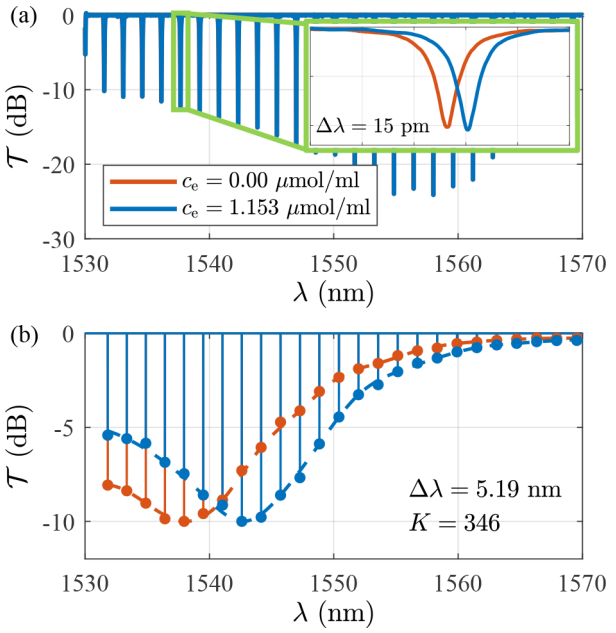

Figure 7. (a) The detected 15 pm spectral shifted resonances for different solutions of metoprolol that can only be seen with a zoom-in. (b) The DSP-generated envelope functions with a sensitivity enhancement factor of 346.

the reference spectra. The sampling comb is now multiplied to each spectrum, yielding the mentioned envelopes. In Figure 7b, an offset of ΔFSR = 10 pm is chosen, yielding an envelope's wavelength shift of 5.19 nm. This corresponds to an enhancement factor of 346 compared to the observation of the spectral resonance shift. The issue of the spectral resolution is circumvented. Nevertheless, any type of spectral shift, including a thermal shift, is enhanced. Thus, the thermal sensitivity limits the achievable LoD to 1×10^{-4} μmol mL^{-1}.

With the assumption that the simulated bulk sensitivity S_n of the photonic MRR (~120 nm RIU^{-1}) matches with extracted uncoated concentration sensitivity S_c of 15 pm ml μmol^{-1}, a refractive index regarded limit of detection can be estimated to $\mathrm{LoD}_n = \mathrm{LoD}_c \times S_c/S_n \sim 2 \times 10^{-8}$ RIU. This is a common metric for biosensors. Together with the material platforms and sensitivities, the presented device can be classified in the state-of-the art selected photonic integrated refractometers operating in the C-band. Table 1 gives an overview of the properties of current state of the art devices used for the detection of solutes such as salts and biomolecules, along with the properties of the devices presented in this work. Well-known photonic devices in the silicon-on-insulator (SOI) and SiN platform are listed as Mach–Zehnder interferometers (MZIs), bimodal waveguide interferometers (BMIs), Bragg gratings, and MRRs. Different methods enable the enhancement of the sensitivity. Impressive numbers of over 50.000 nm/RIU or 60.000 rad/RIU are demonstrated. It has to be mentioned that the different units are legitimized by the fact that either the spectral shift or the change of output power at a single-wavelength were used for detection. Despite those huge values, the limit of detection can be equal or even better for devices with lower sensitivities but better noise suppression. Especially the thermal effect limits the performance. We combined both approaches – a thermally robust architecture and a gaining functional cladding as well as a DSP yielding in a state-of-the-art device. It is important to note that the DSP effect is the only factor considered in the enhancement of sensitivity, which has undergone a substantial increase from 120 nm/RIU to 41,520 nm/RIU. It is hypothesized that if the gain of the functional cladding is also taken into account, sensitivities well surpassing all values collected in Table 1 may be attained.

Table 1. State-of-the-Art Selected Integrated Refractometers Operating in the C-Band[a]

sensor (method)	platform	S_n (RIU^{-1})	LoD_n (RIU)	ref.
MZI (noise suppression)	SiN	4200 rad	1.4×10^{-8}	5
MZI (noise suppression)	SOI	13,051 rad	2.7×10^{-8}	64
BMI (slow light)	SOI	62,900 rad	6.6×10^{-6}	65
BMI in MZI (Vernier)	SOI	51,871 nm		66
BMI (sublambda waveguide)	SOI	2270 nm	2×10^{-5}	67
Sidewall grating (Bragg)	SOI	491 nm		68
MRR (noise suppression)	SOI	113 nm	2.5×10^{-6}	64
MRR (sublambda waveguide)	SOI	490 nm	2×10^{-6}	69
MRR (Vernier)	SOI	24,300 nm		70
MRR (athermal)	SiN	120 nm	2.5×10^{-6}	this work
MRR (athermal + DSP)	SiN	41,520 nm	2×10^{-8}	this work

[a]MZI: Mach–Zehnder interferometer, BMI: bimodal waveguide interferometer.

CONCLUSIONS

In this study, the effect of a hydrogel functional coating on the sensitivity of a silicon nitride photonic chip with an integrated MRR was investigated. As a first step, the adsorption of the drug metoprolol on gelatin methacryloyl hydrogels was characterized. The interaction of metoprolol with the hydrogels, which was described with a modified Langmuir model of adsorption, led to high enrichment of the drug. The characterized hydrogels were thus used to coat the MMR. Characterization of the photonic chip showed high thermal stability. A limit of detection of 0.02 μmol mL^{-1}, which corresponds to 2.5×10^{-6} RIU can be achieved without any hydrogel coating, where the resolution of the laser source sets the limitation. The achieved LoD was found to be similar to LoDs reported for similar devices elsewhere. By calibrating the sensor consisting of a hydrogel coated MRR chip with metoprolol solutions of different concentrations in the range of 0–3 μmol mL^{-1} a significant enhancement of the spectral shift up to a factor of approximately 20 was observed compared to the shifts of the uncoated chip. In this case, a LoD of around 0.001 μmol mL^{-1} is achieved. Utilizing digital signal processing, even a LoD of 1×10^{-4} μmol mL^{-1} can be expected. This value corresponds to an LoD of 2×10^{-8} RIU, which represents the current state-of-the-art with regard to similar photonic devices. The proposed sensor, with its low LoD, represents a straightforward and promising component for the detection of metoprolol, a molecule prevalent in aquatic environments. It is thus contributing to the development of compact sensors that can be used for environmental monitoring purposes.

ASSOCIATED CONTENT

Supporting Information

The Supporting Information is available free of charge at https://pubs.acs.org/doi/10.1021/acsaom.5c00149.

https://doi.org/10.1021/acsaom.5c00149
ACS Appl. Opt. Mater. XXXX, XXX, XXX–XXX

Graphical representation of the chip coating process, ^{1}H NMR spectra of the synthesized GMs, calculation of the hydrogels' water volume fraction, adsorption kinetics, photos of coated chips, Raman spectra of GM and GM hydrogels, MRR transmission spectra with and without coating (PDF)

AUTHOR INFORMATION

Corresponding Authors

Alexander Southan − *Institute of Interfacial Process Engineering and Plasmatechnology IGVP, University of Stuttgart, Stuttgart 70659, Germany; Max Planck Institute for Intelligent Systems, Stuttgart 70569, Germany;* orcid.org/0000-0001-7530-1690; Email: southan@is.mpg.de

Wolfgang Vogel − *Institute of Electrical and Optical Communications Engineering, University of Stuttgart, Stuttgart 70569, Germany;* orcid.org/0000-0002-0611-5365; Email: wolfgang.vogel@int.uni-stuttgart.de

Günter E. M. Tovar − *Institute of Interfacial Process Engineering and Plasmatechnology IGVP, University of Stuttgart, Stuttgart 70659, Germany; Fraunhofer Institute for Interfacial Process Engineering and Biotechnology IGB, Stuttgart 70569, Germany*; Email: guenter.tovar@igvp.uni-stuttgart.de

Authors

Anastasia Tsianaka − *Institute of Interfacial Process Engineering and Plasmatechnology IGVP, University of Stuttgart, Stuttgart 70659, Germany*

Christian Schweikert − *Institute of Electrical and Optical Communications Engineering, University of Stuttgart, Stuttgart 70569, Germany*

Niklas Hoppe − *Institute of Electrical and Optical Communications Engineering, University of Stuttgart, Stuttgart 70569, Germany; Q.ANT GmbH, Stuttgart 70565, Germany*

Markus Greul − *Institut für Mikroelektronik Stuttgart (IMS CHIPS), Stuttgart 70569, Germany*

Mathias Kaschel − *Institut für Mikroelektronik Stuttgart (IMS CHIPS), Stuttgart 70569, Germany*

Manfred Berroth − *Institute of Electrical and Optical Communications Engineering, University of Stuttgart, Stuttgart 70569, Germany*

Georg Rademacher − *Institute of Electrical and Optical Communications Engineering, University of Stuttgart, Stuttgart 70569, Germany*

Complete contact information is available at: https://pubs.acs.org/10.1021/acsaom.5c00149

Author Contributions

‡A.T. and C.S. contributed equally to the work. Conceptualization: A.T., C.S., A.S., N.H., W.V.; Investigation: A.T., C.S.; Data analysis and visualization: A.T., C.S.; Writing (original draft): A.T., C.S.; Writing (review and editing): A.S., N.H., W.V., M.B., G.E.M.T., G.R.; Supervision: A.S., N.H., W.V., M.B., G.E.M.T., G.R.; Resources: M.G., M.K., M.B., G.E.M.T., G.R. All authors have given permission for the final version of the manuscript.

Funding

This work was supported by the Deutsche Forschungsgemeinschaft (DFG) within the project SOSAS (grant ID TO 211/4−1 and BE 2256/37−1). The work of A.S. was partly funded by the Max Planck Society. Open access funded by Max Planck Society.

Notes

The authors declare no competing financial interest.

ABBREVIATIONS

DSP, digital signal processing; ER, extinction ratio; FSR, free spectral range; GM, gelatin methacryloyl; HPLC, high performance liquid chromatography; LoD, limit of detection; MRR, microring resonator; RI, refractive index; RIU, refractive index units

REFERENCES

(1) Prieto, F.; Sepúlveda, B.; Calle, A.; Llobera, A.; Domínguez, C.; Abad, A.; Montoya, A.; Lechuga, L. M. An Integrated Optical Interferometric Nanodevice Based on Silicon Technology for Biosensor Applications. *Nanotechnology* **2003**, *14* (8), 907−912.

(2) Bogaerts, W.; De Heyn, P.; Van Vaerenbergh, T.; De Vos, K.; Kumar Selvaraja, S.; Claes, T.; Dumon, P.; Bienstman, P.; Van Thourhout, D.; Baets, R. Silicon Microring Resonators. *Laser & Photonics Reviews* **2012**, *6* (1), 47−73.

(3) Bassols-Cornudella, B.; Ramirez-Priego, P.; Soler, M.; Estévez, M. C.; Luis-Ravelo, H. J. D.; Cardenosa-Rubio, M.; Lechuga, L. M. Novel Sensing Algorithm for Linear Read-Out of Bimodal Waveguide Interferometric Biosensors. *Journal of Lightwave Technology* **2022**, *40* (1), 237−244.

(4) Schweikert, C.; Tsianaka, A.; Hoppe, N.; Klenk, R. H.; Elster, R.; Greul, M.; Kaschel, M.; Southan, A.; Vogel, W.; Berroth, M. Integrated Polarization Mode Interferometer in 220-Nm Silicon-on-Insulator Technology. *Opt. Lett.* **2022**, *47* (17), 4536−4539.

(5) Leuermann, J.; Fernández-Gavela, A.; Torres-Cubillo, A.; Postigo, S.; Sánchez-Postigo, A.; Lechuga, L. M.; Halir, R.; Molina-Fernández, í. Optimizing the Limit of Detection of Waveguide-Based Interferometric Biosensor Devices. *Sensors* **2019**, *19* (17), 3671.

(6) Gounaridis, L.; Groumas, P.; Schreuder, E.; Tsekenis, G.; Marousis, A.; Heideman, R.; Avramopoulos, H.; Kouloumentas, C. High Performance Refractive Index Sensor Based on Low Q-Factor Ring Resonators and FFT Processing of Wavelength Scanning Data. *Opt. Express* **2017**, *25* (7), 7483−7495.

(7) Chakravarty, S.; Hosseini, A.; Xu, X.; Zhu, L.; Zou, Y.; Chen, R. T. Analysis of Ultra-High Sensitivity Configuration in Chip-Integrated Photonic Crystal Microcavity Bio-Sensors. *Appl. Phys. Lett.* **2014**, *104* (19), No. 191109.

(8) Bryan, M. R.; Butt, J. N.; Ding, Z.; Tokranova, N.; Cady, N.; Piorek, B.; Meinhart, C.; Tice, J.; Miller, B. L. A Multiplex "Disposable Photonics" Biosensor Platform and Its Application to Antibody Profiling in Upper Respiratory Disease. *ACS Sensors* **2024**, *9* (4), 1799−1808.

(9) Yan, H.; Yang, C. J.; Tang, N.; Zou, Y.; Chakravarty, S.; Roth, A.; Chen, R. T. Specific Detection of Antibiotics by Silicon-on-Chip Photonic Crystal Biosensor Arrays. *IEEE Sensors Journal* **2017**, *17* (18), 5915−5919.

(10) Makarona, E.; Petrou, P.; Kakabakos, S.; Misiakos, K.; Raptis, I. Point-of-Need Bioanalytics Based on Planar Optical Interferometry. *Biotechnol Adv.* **2016**, *34* (3), 209−233.

(11) Melnik, E.; Strasser, F.; Muellner, P.; Heer, R.; Mutinati, G. C.; Koppitsch, G.; Lieberzeit, P.; Laemmerhofer, M.; Hainberger, R. Surface Modification of Integrated Optical MZI Sensor Arrays Using Inkjet Printing Technology. *Procedia Engineering* **2016**, *168*, 337−340.

(12) Baillieul, M.; Rinnert, E.; Lemaitre, J.; Michel, K.; Colas, F.; Bodiou, L.; Demésy, G.; Kakuta, S.; Rumyantseva, A.; Lerondel, G.; Boukerma, K.; Renversez, G.; Toury, T.; Charrier, J.; Nazabal, V.

https://doi.org/10.1021/acsaom.5c00149
ACS Appl. Opt. Mater. XXXX, XXX, XXX−XXX

Surface Functionalization with Polymer Membrane or SEIRA Interface to Improve the Sensitivity of Chalcogenide-Based Infrared Sensors Dedicated to the Detection of Organic Molecules. *ACS Omega* **2022**, *7* (51), 47840−47850.
(13) Gorai, P.; Kumar, S.; Marques, C.; Singh, P. K.; Jha, R. Imprinted Polymer Functionalized Concatenated Optical Microfiber: Hypersensitive and Selective. *IEEE Sensors Journal* **2023**, *23* (1), 329−336.
(14) Wang, Y.; Huang, C.-J.; Jonas, U.; Wei, T.; Dostalek, J.; Knoll, W. Biosensor Based on Hydrogel Optical Waveguide Spectroscopy. *Biosens. Bioelectron.* **2010**, *25* (7), 1663−1668.
(15) Hoppe, N.; Föhn, T.; Diersing, P.; Scheck, P.; Vogel, W.; Rosa, M. F.; Kaschel, M.; Bach, M.; Berroth, M. Design of an Integrated Dual-Mode Interferometer on 250 Nm Silicon-on-Insulator. *IEEE J. Sel. Top. Quantum Electron.* **2017**, *23* (2), 444−451.
(16) Alemán, J. V.; Chadwick, A. V.; He, J.; Hess, M.; Horie, K.; Jones, R. G.; Kratochvíl, P.; Meisel, I.; Mita, I.; Moad, G.; Penczek, S.; Stepto, R. F. T. Definitions of Terms Relating to the Structure and Processing of Sols, Gels, Networks, and Inorganic-Organic Hybrid Materials (IUPAC Recommendations 2007). *Pure Appl. Chem.* **2007**, *79* (10), 1801−1829.
(17) Grübel, J.; Wendlandt, T.; Urban, D.; Jauch, C. O.; Wege, C.; Tovar, G. E. M.; Southan, A. Soft Sub-Structured Multi-Material Biosensor Hydrogels with Enzymes Retained by Plant Viral Scaffolds. *Macromol. Biosci.* **2024**, *24* (3), No. 2300311.
(18) Buenger, D.; Topuz, F.; Groll, J. Hydrogels in Sensing Applications. *Prog. Polym. Sci.* **2012**, *37* (12), 1678−1719.
(19) Fortunato, A.; Mba, M. A Peptide-Based Hydrogel for Adsorption of Dyes and Pharmaceuticals in Water Remediation. *Gels* **2022**, *8* (10), 672.
(20) Mandal, B.; Ray, S. K. Removal of Safranine T and Brilliant Cresyl Blue Dyes from Water by Carboxy Methyl Cellulose Incorporated Acrylic Hydrogels: Isotherms, Kinetics and Thermodynamic Study. *Journal of the Taiwan Institute of Chemical Engineers* **2016**, *60*, 313−327.
(21) Li, J.; Mooney, D. J. Designing Hydrogels for Controlled Drug Delivery. *Nature Reviews Materials* **2016**, *1* (12), 16071.
(22) Mealy, J. E.; Rodell, C. B.; Burdick, J. A. Sustained Small Molecule Delivery from Injectable Hyaluronic Acid Hydrogels through Host−Guest Mediated Retention. *J. Mater. Chem. B* **2015**, *3* (40), 8010−8019.
(23) Peers, S.; Montembault, A.; Ladavière, C. Chitosan Hydrogels for Sustained Drug Delivery. *J. Controlled Release* **2020**, *326*, 150−163.
(24) Li, X.; Sun, Q.; Li, Q.; Kawazoe, N.; Chen, G. Functional Hydrogels With Tunable Structures and Properties for Tissue Engineering Applications. *Front. Chem.* **2018**, *6*, 499.
(25) Lee, J.; Lee, H.; Jin, E.-J.; Ryu, D.; Kim, G. H. 3D Bioprinting Using a New Photo-Crosslinking Method for Muscle Tissue Restoration. *npj. Regenerative Medicine* **2023**, *8* (1), 18.
(26) Majer, G.; Southan, A. Adenosine Triphosphate Diffusion through Poly(Ethylene Glycol) Diacrylate Hydrogels Can Be Tuned by Cross-Link Density as Measured by PFG-NMR. *J. Chem. Phys.* **2017**, *146* (22), No. 225101.
(27) Li, H.; Ma, T.; Zhang, M.; Zhu, J.; Liu, J.; Tan, F. Fabrication of Sulphonated Poly(Ethylene Glycol)-Diacrylate Hydrogel as a Bone Grafting Scaffold. *J. Mater. Sci.: Mater. Med.* **2018**, *29* (12), 187.
(28) Sakai, S.; Hirose, K.; Taguchi, K.; Ogushi, Y.; Kawakami, K. An Injectable, in Situ Enzymatically Gellable, Gelatin Derivative for Drug Delivery and Tissue Engineering. *Biomaterials* **2009**, *30* (20), 3371−3377.
(29) Thongrom, B.; Dimde, M.; Schedler, U.; Haag, R. Thiol-Click Based Polyglycerol Hydrogels as Biosensing Platform with In Situ Encapsulated Streptavidin Probes. *Macromol. Chem. Phys.* **2023**, *224* (1), No. 2200271.
(30) İsmail, O.; Gökçe Kocabay, Ö. Absorption and Adsorption Studies of Polyacrylamide/Sodium Alginate Hydrogels. *Colloid Polym. Sci.* **2021**, *299* (5), 783−796.
(31) Liu, T.; Xie, Z. H.; Zhang, Y.; Fan, J.; Liu, Q. Preparation of Cationic Polymeric Nanoparticles as an Effective Adsorbent for Removing Diclofenac Sodium from Water. *Rsc Adv.* **2017**, *7* (61), 38279−38286.
(32) Tang, H.; Zhou, W.; Zhang, L. Adsorption Isotherms and Kinetics Studies of Malachite Green on Chitin Hydrogels. *Journal of Hazardous Materials* **2012**, *209−210*, 218−225.
(33) Chowdhury, N.; Solaiman; Roy, C. K.; Firoz, S. H.; Foyez, T.; Imran, A. B. Role of Ionic Moieties in Hydrogel Networks to Remove Heavy Metal Ions from Water. *ACS Omega* **2021**, *6* (1), 836−844.
(34) Tong, D.; Fang, K.; Yang, H.; Wang, J.; Zhou, C.; Yu, W. Efficient Removal of Copper Ions Using a Hydrogel Bead Triggered by the Cationic Hectorite Clay and Anionic Sodium Alginate. *Environmental Science and Pollution Research* **2019**, *26* (16), 16482−16492.
(35) Jeon, Y. S.; Lei, J.; Kim, J.-H. Dye Adsorption Characteristics of Alginate/Polyaspartate Hydrogels. *Journal of Industrial and Engineering Chemistry* **2008**, *14* (6), 726−731.
(36) Wang, W.; Hu, J.; Zhang, R.; Yan, C.; Cui, L.; Zhu, J. A pH-Responsive Carboxymethyl Cellulose/Chitosan Hydrogel for Adsorption and Desorption of Anionic and Cationic Dyes. *Cellulose* **2021**, *28* (2), 897−909.
(37) Grübel, J.; Albernaz, V. L.; Tsianaka, A.; Jauch, C. O.; Quirin, S.; Kerger, C.; Kohl, C. G.; Burger-Kentischer, A.; Tovar, G. E. M.; Southan, A. Preparation of Multifunctional Hydrogels with Accessible Isothiouronium Groups via Radical Cross-Linking Copolymerization. *Sci. Rep.* **2023**, *13* (1), 10361.
(38) Southan, A.; Tan, J.; Schuster, F.; Rotenberger, J.; Tovar, G. E. M. Adsorption on Inkjet-Printable Polyelectrolyte Hydrogels Allows Refractive Index Sensing of Diclofenac and Metoprolol in Aqueous Solution. *ACS Applied Polymer Materials* **2024**, *6*, 6010.
(39) Dehli, F.; Poole, H.; Stubenrauch, C.; Southan, A. Gelatin-Based Foamed and Non-Foamed Hydrogels for Sorption and Controlled Release of Metoprolol. *ACS Applied Polymer Materials* **2021**, *3* (11), 5674−5682.
(40) Tsianaka, A.; Fichtel, K.; Tovar, G. E. M.; Southan, A. Simultaneous Selective and Quantitative Sensing of Diclofenac and Metoprolol via Electrical Conductance of Two Polyelectrolyte Hydrogels. *Adv. Sens. Res.* **2025**, *4*, No. 2400141.
(41) Yi, M.; Sheng, Q.; Sui, Q.; Lu, H. β-Blockers in the Environment: Distribution, Transformation, and Ecotoxicity. *Environ. Pollut.* **2020**, *266*, No. 115269.
(42) Hoch, E.; Schuh, C.; Hirth, T.; Tovar, G. E.; Borchers, K. Stiff Gelatin Hydrogels Can Be Photo-Chemically Synthesized from Low Viscous Gelatin Solutions Using Molecularly Functionalized Gelatin with a High Degree of Methacrylation. *J. Mater. Sci. Mater. Med.* **2012**, *23* (11), 2607−2617.
(43) Van Den Bulcke, A. I.; Bogdanov, B.; De Rooze, N.; Schacht, E. H.; Cornelissen, M.; Berghmans, H. Structural and Rheological Properties of Methacrylamide Modified Gelatin Hydrogels. *Biomacromolecules* **2000**, *1* (1), 31−38.
(44) Claassen, C.; Claassen, M. H.; Truffault, V.; Sewald, L.; Tovar, G. E. M.; Borchers, K.; Southan, A. Quantification of Substitution of Gelatin Methacryloyl: Best Practice and Current Pitfalls. *Biomacromolecules* **2018**, *19* (1), 42−52.
(45) Karger, B. L. HPLC: Early and Recent Perspectives. *J. Chem. Educ.* **1997**, *74* (1), 45.
(46) Papageorgiou, S. K.; Katsaros, F. K.; Kouvelos, E. P.; Kanellopoulos, N. K. Prediction of Binary Adsorption Isotherms of Cu2+, Cd2+ and Pb2+ on Calcium Alginate Beads from Single Adsorption Data. *Journal of Hazardous Materials* **2009**, *162* (2), 1347−1354.
(47) Gulsen, D.; Chauhan, A. Effect of Water Content on Transparency, Swelling, Lidocaine Diffusion in p-HEMA Gels. *J. Membr. Sci.* **2006**, *269* (1), 35−48.
(48) Dursch, T. J.; Taylor, N. O.; Liu, D. E.; Wu, R. Y.; Prausnitz, J. M.; Radke, C. J. Water-Soluble Drug Partitioning and Adsorption in HEMA/MAA Hydrogels. *Biomaterials* **2014**, *35* (2), 620−629.

https://doi.org/10.1021/acsaom.5c00149
ACS Appl. Opt. Mater. XXXX, XXX, XXX−XXX

(49) Arbabi, A.; Goddard, L. L. Measurements of the Refractive Indices and Thermo-Optic Coefficients of Si3N4 and SiOx Using Microring Resonances. *Opt. Lett.* **2013**, *38* (19), 3878−3881.
(50) Kim, Y. H.; Park, S. J.; Jeon, S.-W.; Ju, S.; Park, C.-S.; Han, W.-T.; Lee, B. H. Thermo-Optic Coefficient Measurement of Liquids Based on Simultaneous Temperature and Refractive Index Sensing Capability of a Two-Mode Fiber Interferometric Probe. *Opt. Express* **2012**, *20* (21), 23744−23754.
(51) Erben, A.; Hörning, M.; Hartmann, B.; Becke, T.; Eisler, S. A.; Southan, A.; Cranz, S.; Hayden, O.; Kneidinger, N.; Königshoff, M.; Lindner, M.; Tovar, G. E. M.; Burgstaller, G.; Clausen-Schaumann, H.; Sudhop, S.; Heymann, M. Precision 3D-Printed Cell Scaffolds Mimicking Native Tissue Composition and Mechanics. *Adv. Healthcare Mater.* **2020**, *9* (24), No. 2000918.
(52) Ghosh, R. N.; Thomas, J.; Videhi, B. R.; Devi, N. G.; Janardanan, A.; Namboothiri, P. K.; Peter, M. An Insight into Synthesis, Properties and Applications of Gelatin Methacryloyl Hydrogel for 3D Bioprinting. *Mater. Adv.* **2023**, *4* (22), 5496−5529.
(53) Yue, K.; Trujillo-de Santiago, G.; Alvarez, M. M.; Tamayol, A.; Annabi, N.; Khademhosseini, A. Synthesis, Properties, and Biomedical Applications of Gelatin Methacryloyl (GelMA) Hydrogels. *Biomaterials* **2015**, *73*, 254−271.
(54) Vigata, M.; O'Connell, C. D.; Cometta, S.; Hutmacher, D. W.; Meinert, C.; Bock, N. Gelatin Methacryloyl Hydrogels for the Localized Delivery of Cefazolin. *Polymers* **2021**, *13* (22), 3960.
(55) Jiang, D.; Ge, P.; Wang, L.; Jiang, H.; Yang, M.; Yuan, L.; Ge, Q.; Fang, W.; Ju, X. A Novel Electrochemical Mast Cell-Based Paper Biosensor for the Rapid Detection of Milk Allergen Casein. *Biosens. Bioelectron.* **2019**, *130*, 299−306.
(56) Claassen, C.; Southan, A.; Grubel, J.; Tovar, G. E. M.; Borchers, K. Interactions of Methacryloylated Gelatin and Heparin Modulate Physico-Chemical Properties of Hydrogels and Release of Vascular Endothelial Growth Factor. *Biomed Mater.* **2018**, *13* (5), No. 055008.
(57) Rebers, L.; Reichsöllner, R.; Regett, S.; Tovar, G. E. M.; Borchers, K.; Baudis, S.; Southan, A. Differentiation of Physical and Chemical Cross-Linking in Gelatin Methacryloyl Hydrogels. *Sci. Rep.* **2021**, *11* (1), 3256.
(58) Vassallo, V.; Tsianaka, A.; Alessio, N.; Grübel, J.; Cammarota, M.; Tovar, G. E. M.; Southan, A.; Schiraldi, C. Evaluation of Novel Biomaterials for Cartilage Regeneration Based on Gelatin Methacryloyl Interpenetrated with Extractive Chondroitin Sulfate or Unsulfated Biotechnological Chondroitin. *J. Biomed. Mater. Res., Part A* **2022**, *110* (6), 1210−1223.
(59) Nazarova, O. V.; Panarin, E. F.; Kuznetsov, L. L.; Zavlin, P. M. Methacryloyl Derivatives of Gelatin and Copolymers Based on Them. *Russ. J. Appl. Chem.* **1994**, *67* (4), 623−624.
(60) Sewald, L.; Claassen, C.; Gotz, T.; Claassen, M. H.; Truffault, V.; Tovar, G. E. M.; Southan, A.; Borchers, K. Beyond the Modification Degree: Impact of Raw Material on Physicochemical Properties of Gelatin Type A and Type B Methacryloyls. *Macromol. Biosci* **2018**, *18* (12), No. e1800168.
(61) Luan, E.; Shoman, H.; Ratner, D. M.; Cheung, K. C.; Chrostowski, L. Silicon Photonic Biosensors Using Label-Free Detection. *Sensors* **2018**, *18* (10), 3519.
(62) Schweikert, C.; Klenk, R. H.; Winkel, S.; Hoppe, N.; Vogel, W.; Berroth, M.; Rademacher, G. Thermally Robust Silicon Integrated Ring Resonators With Postprocessing Sensitivity Enhancement for Biosensing. *J. Lightwave Technol.* **2025**, *43*, 4819−4825.
(63) Kazakov, D.; Letsou, T. P.; Beiser, M.; Zhi, Y.; Opačak, N.; Piccardo, M.; Schwarz, B.; Capasso, F. Active Mid-Infrared Ring Resonators. *Nature. Communications* **2024**, *15* (1), 607.
(64) van Gulik, R. J. J.; de Boer, B. M.; Harmsma, P. J. Refractive Index Sensing Using a Three-Port Interferometer and Comparison With Ring Resonators. *IEEE J. Sel. Top. Quantum Electron.* **2017**, *23* (2), 433−439.
(65) Torrijos-Morán, L.; Griol, A.; García-Rupérez, J. Slow Light Bimodal Interferometry in One-Dimensional Photonic Crystal Waveguides. *Light: Science & Applications* **2021**, *10* (1), 16.
(66) Zhang, Y.; Wang, L.; Yao, H.; Deng, J.; Wu, J.; Zhao, Z.; Chen, K. Ultrahigh-Sensitivity Liquid Refractive Index Sensor with Two-Mode Interferometer Embedded in Each Arm of Mach-Zehnder Interferometer. *Journal of Lightwave Technology* **2025**, 1−7.
(67) Torrijos-Morán, L.; Griol, A.; García-Rupérez, J. Experimental Study of Subwavelength Grating Bimodal Waveguides as Ultrasensitive Interferometric Sensors. *Opt. Lett.* **2019**, *44* (19), 4702−4705.
(68) di Toma, A.; Brunetti, G.; Colapietro, P.; Ciminelli, C. High-Resolved Near-Field Sensing by Means of Dielectric Grating With a Box-Like Resonance Shape. *IEEE Sens. J.* **2024**, *24* (5), 6045−6053.
(69) Flueckiger, J.; Schmidt, S.; Donzella, V.; Sherwali, A.; Ratner, D. M.; Chrostowski, L.; Cheung, K. C. Sub-Wavelength Grating for Enhanced Ring Resonator Biosensor. *Opt. Express* **2016**, *24* (14), 15672−15686.
(70) Jiang, X.; Ye, J.; Zou, J.; Li, M.; He, J.-J. Cascaded Silicon-on-Insulator Double-Ring Sensors Operating in High-Sensitivity Transverse-Magnetic Mode. *Opt. Lett.* **2013**, *38* (8), 1349−1351.

https://doi.org/10.1021/acsaom.5c00149
ACS Appl. Opt. Mater. XXXX, XXX, XXX−XXX